Cooperative Path-Following Control of Aerial and Marine Vehicles

António Manuel Fernandes de Sousa Antunes
antonioantunes5@tecnico.ulisboa.pt

Instituto Superior Técnico, Lisboa, Portugal

Abstract

This master's dissertation deals with a cooperative mission between an aerial and a marine vehicle connected by a tether. The tether is modelled as a cable with two suspension points and the corresponding equilibrium condition is studied. Subsequently, an analysis is made regarding the management of the cable length in order to allow the success of the mission, minimizing its impact on the vehicles and on the cable itself. This analysis converges to a function capable of computing the ideal length for the cable depending on the relative position of the vehicles. Next, to pave the way for the development of cooperation while following paths, models for the two types of vehicles are presented, as well as methods of controlling them. For the aerial vehicle, a hierarchical structure is adopted with an inner loop to control the orientation and an outer loop to control the translation movement. As far as the marine vehicle is concerned, two inner loops are used for the surge speed and the yaw rate. The Cooperative Path-following (CPF) is achieved through the use of a virtual target, as a facilitator of references for each vehicle. These targets are coordinated by a continuous synchronization protocol. Finally, results are presented in the form of simulations, first of each vehicle individually and then of both in formation interconnected by the cable. A plug-in is also introduced, in the context of a mission in Robot Operating System (ROS), created to incorporate a simulated cable in the Gazebo simulator.
Keywords: Unmanned Aerial Vehicle, Autonomous Surface Vehicle, Tether, Cooperative Path-following.

I. Introduction

I-A. Motivation and Problem Definition

This Master's dissertation addresses the problem of "Cooperative Path-Following Control of Aerial and Marine Vehicles". More specifically, the work is focused on studying cooperative scenarios where an unmanned aerial vehicle Unmanned Aerial Vehicle (UAV) and an autonomous surface vehicle Autonomous Surface Vehicle (ASV) are linked by a tether as presented in figure 1.

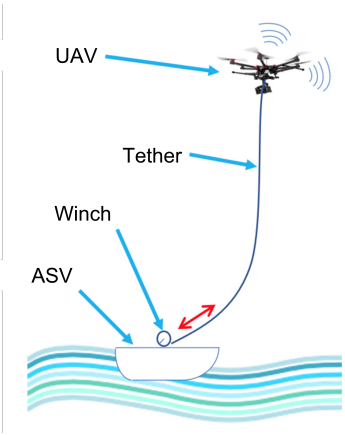

Fig. 1: Representation of an UAV and an ASV linked by a tether. (adopted from [11]).

The cooperation between vehicles in certain environments can be a great way of increasing the performance and success rate of any mission. It also allows for the execution of more complex missions, for example, tasks that require two agents in two different locations at the same time. However, there is a big differentiating factor between both vehicles, which is autonomy. The aerial vehicles, electric multirotors, have typically an autonomy below 30 minutes. The proposed solution, as previously stated, is the use of a tether as a power supply linking the two vehicles. The use of this type of link also provides a line of communication between the two agents. There is no need to attach data storage systems to the aerial vehicle, reducing its weight which will naturally lead to a potential improvement in performance. There are already some offers of tethered drones in the market. Nonetheless, these offers tend to be for static situations such as live detection of natural disasters, subsequent monitoring and possible humanitarian support, road traffic control, increase of the range of telecommunication networks, video surveillance systems for example with the purpose of security of private property or even for crowd control, image collection and data acquisition, the list goes on. The goal is to offer the same possibilities but in a dynamic mode, instead of being fixed to a ground base station. In this mode, new possibilities emerge, for example, the surveillance and the detection of natural disasters can now be done by a single

itinerant aircraft instead of a formation of fixed location ones. Another example integrated into the maritime context is the coastal patrol, which with a system of this kind can monitor a much larger area without an autonomy constraint. There is a condition for this approach to be effective, which has to do with the clearance of the environment in question: there is no room for obstacles that hinder the existence of the cable that connects the two agents. Another limitation is the length of the tether which can reduce the range of action of the drone. In academic terms, this approach is interesting from a control point of view because it is necessary to frame two completely different entities in terms of their dynamics and characteristics and design a controller capable of following a path while, at the same time, knowing how to deal with the disturbance caused by the cable in the aerial vehicle.

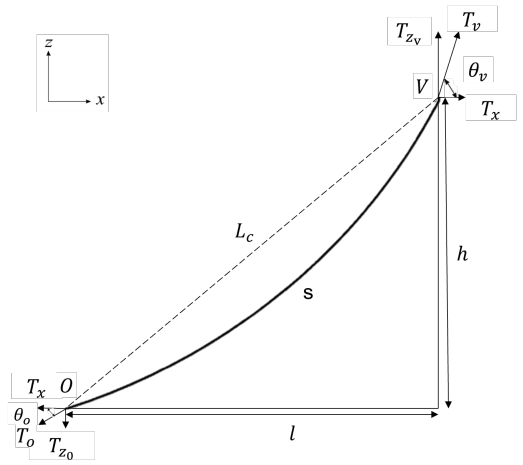

Fig. 2: Free-body diagram illustrating a fully-elevated tether.

II. Tether - Modelling and Dynamic Operation

II-A. Tether Model

There are three types of forces exerted on a tether in this scenario, a cooperative mission between an aerial and a marine surface vehicle linked by such a structure. Those forces are the cable's weight, the aerodynamic drag force and the tension forces caused by its interaction with the vehicles.

II-A1 Tether Equilibrium

The tether behaviour can be described through several moments, the take-off, the flight in which both vehicles move across space simultaneously, waypoint tasks in which the ASV is in a fixed location and the UAV may move within its flight envelope to perform any kind of mission and landing. In all of these situations, the tether will be modelled in a fully-elevated state through quasi-static catenary equations as it is in [5]. A free-body diagram illustrating the system in study is in figure 2.

A function of z in order to x can be defined as

$$z(x) = \frac{T_x}{\mu_t} \cosh\left(\frac{\mu_t}{T_x} x + C_1\right) + C_2. \tag{1}$$

In this situation, a tether describes a well-known shape: the catenary. The equation (1) is the catenary equation adapted to this problem. The constants C_1 and C_2 will allow the catenary to no longer be a generic shape but to be exactly where it is supposed to be between the two tether fixed extremities. Then the expressions for the values of both the mentioned constants and T_x will be determined, given the coordinates of the hanging points and the length of the cable. These two points are $(0, 0)$, considering the origin of the referential as the ASV connection to the tether, and (l, h) as the UAV connection to the tether. By using the point $(0, 0)$ it is possible to get

$$C_2 = -\frac{T_x}{\mu_t} \cosh(C_1). \tag{2}$$

With the point (l, h) and with the equation (2) the other constant is derived,

$$C_1 = \sinh^{-1}\left(\frac{\mu_t h}{2T_x \sinh(\frac{\mu_t l}{2T_x})}\right) - \frac{\mu_t l}{2T_x}. \tag{3}$$

The angles of departure of the tether in both vehicles are

$$\theta_O = tan^{-1}(\sinh(C_1)), \tag{4}$$

$$\theta_V = tan^{-1}\left(\sinh\left(\frac{\mu_t l}{T_x} + C_1\right)\right). \tag{5}$$

The vertical force exerted by the tether on each hanging point is

$$T_{z_O} = T_x tan\theta_O, \tag{6}$$

$$T_{z_V} = T_x tan\theta_V. \tag{7}$$

To compute the applied torque by the tether on the aircraft with

$$\tau_V = S(f) R^T T_V, \tag{8}$$

where R^T is the orientation of the axis of the body-fixed frame with respect to the body-fixed reference frame which is given by ${}^B_I R \in \mathbb{SO}^3$, f is the mounting point of the tether on the UAV on its body-frame and $S(f)$ its respective skew-matrix.

A zero function is to be defined to compute the horizontal reaction force T_x

$$f_0 = \frac{2T_{x_n}}{\mu_t} \sinh\left(\frac{\mu_t l}{2T_{x_n}}\right) - \sqrt{L_t^2 - h^2}. \tag{9}$$

To compute the horizontal reaction force T_x a numerical method, the Newton Method is used

since f_0 is a transcendental equation which cannot be turned into an algebraic one. The method consists of iteratively approximating the roots of a zero function f_0 and by doing that finding a good estimate for the horizontal force T_x. The method is described by

$$T_{x_{n+1}} = T_{x_n} - \frac{f_0}{\frac{\partial f_0}{\partial T_{x_n}}}. \tag{10}$$

An initial estimate for T_{x_n} can be

$$T_{x_0} = \frac{\mu_t l}{2x}, \tag{11}$$

which improves the method's performance.

II-A2 Tether Dynamics

Despite being considered a quasi-static scenario to define the tether governing equations, in which it is always very close to equilibrium either in terms of shape or tension. One needs always to account for the dynamics which, especially in extreme scenarios, may lead to relevant disturbances in the tether and finally in the whole system.

In [5] the tether is seen as a string, whose possible disturbances are oscillatory in nature. There are two types of waves in a string, the longitudinal which acts tangentially to the tether and the transversal which are perpendicular to the tether. Those two types of waves may exist due to only two agents, aerodynamic forces and the UAV. Any disturbance that reaches the fundamental frequency or its harmonics can resonate and create a high-amplitude wave, that might be harmful to the system in particular for the UAV.

II-B. Flying Space

To connect a tether between an ASV and an UAV in a marine scenario there are some constraints that one needs to take into account.

1) The tether must not get in the water. This means that if its departure point in the ASV, in the worst-case scenario, is barely at the water's level its departure angle has to be bigger or equal to zero degrees.
2) The distance between the UAV and the ASV must always be smaller or equal to the tether maximum length. In practice, the vehicles should operate within some distance from this borderline scenario. This is another event to account for when designing the safety measures mentioned above.
3) The tension exerted by the tether in the UAV must never surpass its maximum thrust. It is a good practice to have a margin between this maximum achievable tension and the maximum thrust of the vehicle. The aerial vehicle can be protected regarding this concern at an early stage of the implementation by selecting a tether whose weight is fully supported by the UAV with some thrust to spare. On the other hand, it is also good practice to prevent the cable from being fully stretched, it can lead to the UAV trying to move farther away with an increasingly bigger cost. Forcing against the maximum length of the tether can ultimately lead to unnecessary spending of energy by the aerial vehicle or, in the worst-case scenario, breaking the link between the vehicles. This is very similar to what was mentioned in the previous topic which dealt with safety measures.

A fully-elevated tether scenario is assumed, in which the cable is completely unrolled vertically during take-off and completely rolled during landing. To fulfil the points presented above there are very few relative positions between the vehicles in which the tether would behave as expected. Those positions are located near the maximum distance points, the hemispherical surface of radius equal to the fixed tether length. This is shown for a tether with a length of 50 m by the 2D discretization of the flying space present in figure 3.

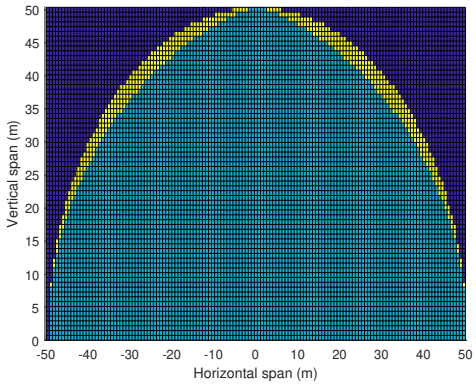

Fig. 3: 2D discretization of the flying space. A position in yellow is a valid position. A position in light blue is invalid due to the tether's departure angle being smaller than zero which means that it contacts with the water. A darker blue position is out of the tether range.

III. Flying Space with a Dynamic Tether Length

The approach is similar to the one in [12], however, adapted to the equilibrium described in previous sections as well as with other choices of values, for example, the value for μ_t is 0.030 kg m^{-1}. For example purposes, the maximum tether length chosen in this section is also 50 m.

The desired working zone is the one that guarantees that the departure angle is always positive, pointing upwards, which is the ultimate goal. However, there are other factors to take into account,

the tension exerted in the UAV should be as low as possible to reduce its disturbance effect and the power consumption. A representation for a fixed relative position $(l, h) = (35, 15)\,m$ the tension exerted by tether at the UAV as a function of the tether length is shown in figure 4.

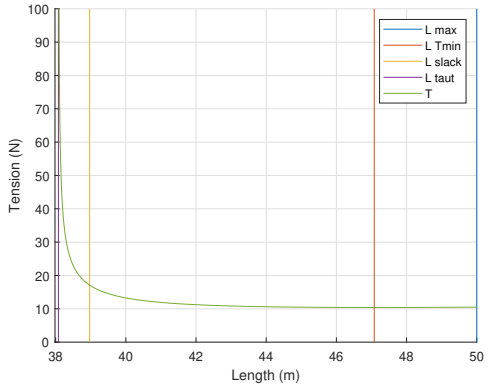

Fig. 4: Tension exerted by the tether in the UAV as a function of the tether length. Notable points are also assigned, maximum length, minimum tension, slack and taut configurations.

Decreasing from the slack length to the taut length leads to increasing tension in the aerial vehicle. The growth rate gets asymptotically bigger, virtually to infinity which is not the reality, as the length tends to the taut length. In [12] it is suggested as viable options to seek lengths that increase the tension on the UAV by 5%, 10% and 20%.

III-A. Polynomial Fit for a Tether Length Function

By re-discretizing the two-dimensional (2D) space as it was done in 3 and computing for each position which length leads to minimum tension, slack, 5%, 10% or 20% increasing tension it is possible to define a polynomial fit of 3^{rd} degree of the data computed for each point in the bi-dimensional space after being normalized through the relative height between vehicles. This approximation consists of finding the coefficients that better fit this expression,

$$L_t = c_1 h + c_2 l + c_3 \frac{l^2}{h} + c_4 \frac{l^3}{h^2}. \qquad (12)$$

The table I has the coefficients and its R^2 corresponding to the confidence in the least squares approximation.

L	c_1	c_2	c_3	c_4	R^2
L_{Tmin}	1.0109	0.1385	0.6348	−0.1575	0.9663
L_{slack}	0.9887	0.2492	0.2898	−0.0437	0.9995
L_5	0.9708	0.2268	0.3142	−0.0498	0.9995
L_{10}	0.9703	0.2012	0.3331	−0.0533	0.9996
L_{20}	0.9727	0.1650	0.3589	−0.0585	0.9997

TABLE I: Coefficients of the polynomial fit of 3^{rd} degree for the length of the tether per unit height that leads to notable scenarios such as minimum tension, slack, 5%, 10% or 20% increasing tension depending on the relative position.

However, these polynomials for bigger relative positions end up becoming useless, this is not shown in the figure even though it happens in the form of an inflexion point, which is expected since it is a third-degree polynomial. The smallest inflexion point is for $l/h \approx 2.05$. A solution can be to use the third-degree polynomial for $l/h \leq 1.95$ and extrapolate for a second-degree polynomial to use when $l/h \geq 2.15$, in between a linear combination of both can be used to smooth the transition.

After the extrapolation is performed it yields the coefficients for the 2^{nd} degree polynomial written in table II.

L	c_1	c_2	c_3	R^2
L_5	0.9594	0.3103	0.1890	0.9998
L_{10}	0.9582	0.2907	0.1990	0.9997
L_{20}	0.9595	0.2630	0.2118	0.9997

TABLE II: Coefficients of the polynomial fit of 2^{nd} degree extrapolated from the 3^{rd} degree polynomial fit for the length of the tether per unit height that leads to notable scenarios such as 5%, 10% or 20% increasing tension in reference to slack tension depending on the relative position.

By using a simple average as the linear combination to smooth the transition between the first fit and the second one it allows the function to compute values for tether lengths in scenarios where the relation between the horizontal span and the vertical span is even bigger than before.

III-B. Heave Tolerance

To compare the heave robustness of the tether in question for the three functions previously defined, a 2D flying space analysis was made for each tension increase, with the upward and downward tolerance for each position represented. The best working zone is one that maximizes both tolerances. As expected the 5% option, because it is closer to slack length, has a better downward motion tolerance, the opposite occurs for the 20% option. The 10% increase from slack tension is the more balanced choice in which generally one can get bigger values for both types of motion as presented in figures 5 and 6. Despite all of this, all three

functions present acceptable working zones, it is up to the designer to choose the one that suits better its system. Is power consumption a problem? Then the tension on UAV shall be minimised by choosing a smaller increase from slack tension, the 5% length function. Is upward motion robustness more important than downward, which may mean that it is more of a priority to avoid contact with the water than to avoid fully stretching the tether? The best choice is the 20% tether length function.

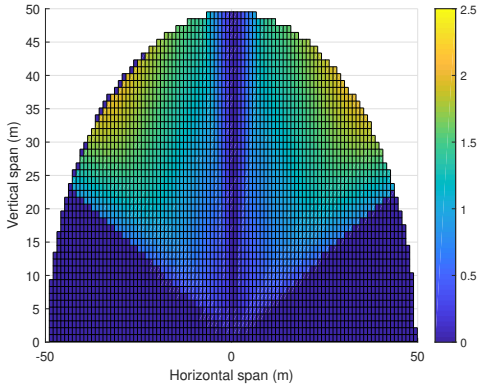

Fig. 5: Upward motion, 10% tension increase from slack tension.

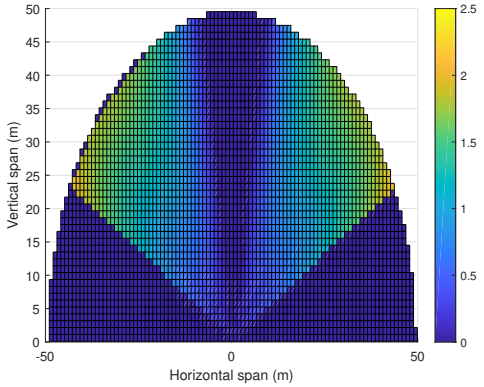

Fig. 6: Upward motion, 10% tension increase from slack tension.

IV. UAV - Modelling and Control

The theoretical foundation of this section is based on the contents present in [9] and [8].

IV-A. Quadrotor Model

There are two important frames: the inertial reference frame {I} which can be fixed anywhere and follows the North-East-Down (NED) convention, and the body-fixed frame {B} which is fixed to the body and follows the same convention. Reference frames are defined by an origin and 3 orthonormal axes. The inertial reference frame $\mathcal{F}_I = \{O_I, \mathrm{x}_I, \mathrm{y}_I, \mathrm{z}_I\}$ and the body-fixed frame $\mathcal{F}_B = \{O_B, \mathrm{x}_B, \mathrm{y}_B, \mathrm{z}_B\}$ are shown in figure 7.

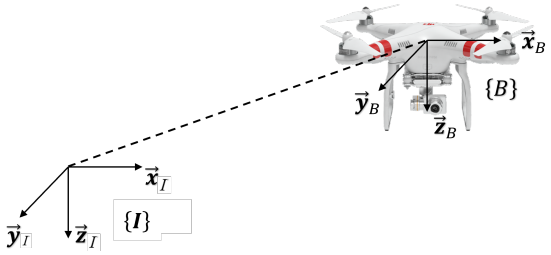

Fig. 7: Inertial reference frame {I} and body-fixed frame {B}.

The position of the origin of the body-fixed frame with respect to the inertial reference frame is given by ${}^{I}p_B \in \mathbb{R}^3$. The orientation of the axis of the body-fixed frame with respect to the inertial reference frame is given by ${}^{I}_{B}R \in \mathbb{SO}(3)$. To simplify the notation consider that $p = {}^{I}p_B$ and $R = {}^{I}_{B}R$.

IV-B. Quadrotor Kinematics

The kinematics of the quadrotor are given by

$$\dot{p} = Rv \tag{13}$$

$$\dot{R} = RS(\omega). \tag{14}$$

where v is the linear velocity and ω the angular velocity, both expressed in the body frame. The $S(\omega)$ is the skew matrix of ω that when multiplied with another vector performs the cross product.

IV-B1 Quadrotor Translational Dynamics

If a near hover condition is considered in which aerodynamic drag is neglected there are only three forces applied to the vehicle, which are its own thrust (T), the gravitational force and any other disturbances, yielding

$${}^{I}f = mge_3 - TRe_3 + T_V + D, \tag{15}$$

where T_V denotes the disturbance created by the tether on the UAV in the inertial frame and D every other disturbance such as the wind. The equation of motion for translation can be written as

$$\ddot{p} = ge_3 - \frac{T}{m}Re_3 + \frac{T_V}{m} + \frac{D}{m}. \tag{16}$$

IV-B2 Quadrotor Rotational Dynamics

The rotational dynamics can be written as

$$J\dot{\omega} = -S(\omega)J\omega + \tau, \tag{17}$$

IV-C. Quadrotor Trajectory Tracking Control

The trajectories to be tracked are defined as position vectors $p_d(t) \in \mathbb{R}^3$ that are sufficiently smooth functions of time such that $\dot{p}_d(t)$ and $\ddot{p}_d(t)$ are well defined for all $t > 0$. This structure is composed of an outer-loop for the translational

dynamics which computes the quadrotor thrust, T, and desired orientation, $R_d e_3$, which in turn feeds the inner-loop which is responsible for controlling the applied torque, τ. Figure 8 presents the control system structure, which is an inner-loop outer-loop control where the inner part shall be faster than its outer part to get the desired stability for the whole system.

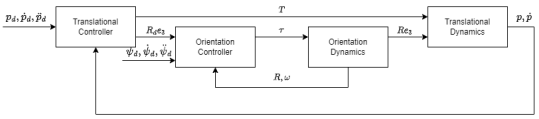

Fig. 8: Block diagram of the quadrotor trajectory tracking control system.

IV-C1 Translational Controller

The control law for u_T in order to follow the translational references is

$$u_T = -K_P\tilde{p}(t) - K_I \int_0^t \tilde{p}(\tau)d\tau - K_D\dot{\tilde{p}}(t) - g + \ddot{p}_d(t), \tag{18}$$

where $\tilde{p}(t) = p(t) - p_d(t)$, and $K_P > 0$, $K_I > 0$ and $K_D > 0$ the system is stable and by means of the integral action $\tilde{p}$ converges to zero even in the presence of constant disturbances T_V and D. The translational dynamics will receive as an input the thrust as a value for the magnitude of the force applied,

$$T = m\|u_T\|. \tag{19}$$

The orientation controller will receive the direction in which the thrust should be applied,

$$R_d e_3 = -\frac{u_T}{\|u_T\|}. \tag{20}$$

IV-C2 Orientation Controller

The control law for τ in order to follow the orientation references is

$$\tau = -K_P\tilde{\lambda}(t) - K_D\dot{\tilde{\lambda}}(t) + \ddot{\lambda}_d(t). \tag{21}$$

where $K_P > 0$ and $K_D > 0$, $\tilde{\lambda}(t) = \lambda(t) - \lambda_d(t)$, $\lambda = (\phi, \theta, \psi)$ and $\lambda_d = (\phi_d, \theta_d, \psi_d)$, in which $\psi_d = 0$ and the pair ϕ_d and θ_d is computed from the desired orientation $R_d e_3$.

V. ASV - Modelling and Control

There are two reference frames, the Inertial reference frame {I} with basis $\mathcal{F}_I = \{O_I, \mathrm{x}_I, \mathrm{y}_I, \mathrm{z}_I\}$, aligned with the NED convention, and the Body-fixed frame {B} with basis $\mathcal{F}_B = \{O_B, \mathrm{x}_B, \mathrm{y}_B, \mathrm{z}_B\}$ which is fixed to the body center of mass, the x_B is the longitudinal axis which is directed from aft to fore, the y_B is the transversal axis which is directed to starboard and z_B is the normal axis which is directed downwards. A representation of both reference frames is presented in figure 9.

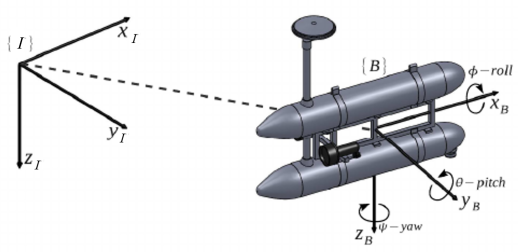

Fig. 9: Inertial reference frame {I} and body-fixed frame {B} (adopted from [10]).

To model a marine vehicle it is necessary to account for its 6 Degrees of freedom (DOF), three coordinates for position (x, y, z), surge, sway and heave, and another three for orientation (ϕ, θ, ψ), roll, pitch and yaw.

V-A. Simplified Equations of Motion

In this section, it is defined a set of equivalent equations, as in [3], specific for the surface case of those vehicles, with all the necessary simplifications. Assuming that the working zone is approximately a 2D plane, which means that there is only 3 DOF which are $[x, y, \psi]^T$, it is considered that $\theta \approx 0\,rad$, $\phi \approx 0\,rad$ and $z \approx 0$. The kinematics of the ASV are,

$$\begin{bmatrix}\dot{x}\\ \dot{y}\end{bmatrix} = \begin{bmatrix}cos(\psi) & -sin(\psi)\\ sin(\psi) & cos(\psi)\end{bmatrix}\begin{bmatrix}u\\ v\end{bmatrix}, \tag{22}$$

$$\dot{\psi} = r. \tag{23}$$

In this equations, u and v are the surge speed and the sway speed, respectively, both in the body-fixed frame, x and y define the 2D position in the inertial frame with ψ defining orientation in the same frame and r the angular speed. If there is a constant and irrotational ocean current $[u_c, v_c]^T \neq 0$, both surge and sway speed are $u = u_r + u_c$ and $v = v_r + v_c$, with u_r and v_r being the relative body-current linear velocities. In what concerns the dynamics, by using the same simplifications, the new equations are,

$$m_u\dot{u}_r - m_v v_r r + d_{u_r}u_r = \tau_u, \tag{24}$$

$$m_v\dot{v}_r + m_u u_r r + d_{v_r}v_r = 0, \tag{25}$$

$$m_r\dot{r} - m_{uv}u_r v_r + d_r r = \tau_r, \tag{26}$$

where the τ_u is the external force in surge motion and τ_r is the external torque along the z axis, and also,

$$\begin{aligned} m_u &= m - X_{\dot{u}}, \quad d_{u_r} = -X_u - X_{|u|u}|u_r|,\\ m_v &= m - Y_{\dot{v}}, \quad d_{v_r} = -Y_v - Y_{|v|v}|v_r|,\\ m_r &= I_z - N_{\dot{r}}, \quad d_r = -N_r - N_{|r|r}|r|,\\ m_{uv} &= m_u - m_v, \end{aligned} \tag{27}$$

with m_u, m_v, m_r and m_{uv} representing the mass and hydrodynamic added mass and d_u, d_v and d_r

being the hydrodynamic damping effects. These set equations assume that the ASV is neutrally buoyant and that its centre of buoyancy coincides with the centre of gravity.

V-B. ASV Control

The proposed control scheme is to control both linear and angular velocities, respectively the surge speed u and the yaw rate r. In this section a control law is derived for each one of the system's inputs, the force along the surge axis τ_u and the torque along the body z-axis, to make $[u, r]^T$ converge to the desired $[u_d, r_d]^T$. The proposed control structure is displayed in figure 10.

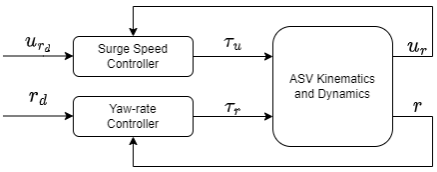

Fig. 10: Block diagram of the ASV control system.

V-B1 Surge Speed Control

It is considered that the sway speed is approximately zero, $v \approx 0$. The control law for τ_u in order to follow the orientation references is

$$\tau_u = m_u \left[-K_P \tilde{u}_r(t) - K_I \int_0^t \tilde{u}_r(\tau) d\tau + \dot{u}_{r_d}(t) \right] + d_{u_r} u_r, \tag{28}$$

where $K_P > 0$ and $K_I > 0$.

V-C. Yaw Rate Control

It is also considered that the sway speed is approximately zero, $v \approx 0$. The control law for τ_r in order to follow the orientation references is

$$\tau_r = m_u \left[-K_P \tilde{r}(t) - K_I \int_0^t \tilde{r}(\tau)\, d\tau + \dot{r}_d(t) \right] + d_r r \tag{29}$$

VI. Cooperative Path-following (CPF)

VI-A. Path-following (PF)

This section follows a strategy that converts Trajectory Tracking (TT) into PF with the help of a virtual target. This creates a less demanding scenario for any vehicle, it is only TT when the vehicle is close to the virtual target, otherwise, the references are updated to improve the vehicle's ability to follow the path. The definition of this virtual target is based on [13] which is about creating two control laws, one to define the virtual target evolution along the pre-defined path and another to define a reference to follow by the vehicle based on the position and motion of the target. The idea is to consider a vehicle with known kinematics and dynamics, and also a virtual target which position is defined by $p_d(\gamma)$, which is $p_d(\gamma) \in \mathbb{R}^2$ for the ASV and $p_d(\gamma) \in \mathbb{R}^3$ for the UAV, with a desired speed of $v_d(\gamma) \in \mathbb{R}$. This position and desired speed are parameterized by $\gamma \in \mathbb{R}$, which represents each instant in time through the trajectory. The goal is to create control laws for u_d and $\dot{\gamma}$, which are the reference speed $[u_d, r_d]^T$ for the ASV and $[p_d, \dot{p}_d, \ddot{p}_d]^T$ for the UAV, and the rate of evolution of the virtual target along the path. Ultimately this laws shall lead to $||p(t) - p_d(\gamma(t))|| \to 0$ and to $\dot{\gamma}(t) \to 1$ as time goes by, $t \to \infty$.

VI-A1 ASV Path-following Control Design

To perform the PF one needs to define the references to track but also the evolution of the virtual target through time. The references are given by

$$u_d = \Delta^{-1} \left(-K_k (\tilde{p} - \boldsymbol{\delta}) - \begin{bmatrix} 0 \\ v \end{bmatrix} + {}^B_I R v_c - {}^B_I R(\psi) \frac{\partial p_d(\gamma)}{\partial \gamma} \dot{\gamma} \right), \tag{30}$$

where $u = [u_r, r]^T$, $\Delta = \left[\begin{smallmatrix} 1 & 0 \\ 0 & -\delta \end{smallmatrix} \right]$, $\boldsymbol{\delta} = [\delta, 0]^T$, $\delta < 0$, $K_k \succeq 0$, $K_k = \left[\begin{smallmatrix} k_x & 0 \\ 0 & k_y \end{smallmatrix} \right]$, v is the sway speed and v_c is the ocean currents speed expressed in the inertial frame. The term $\frac{\partial p_d(\gamma)}{\partial \gamma}$ is the desired velocity for the virtual target assigned to its position in the path. When the error is big the target must move slowly and at some point even stop to wait for the vehicle to get closer to it and therefore converge to the path. The first derivative of the virtual target, $\dot{\gamma}$, is specified as a function of the distance between the vehicle and the target,

$$\dot{\gamma}_{REF} = \begin{cases} 0 & ||p(t) - p_d(\gamma)|| \geq d \\ e^{\frac{||p(t) - p_d(\gamma)||^2}{||p(t) - p_d(\gamma)||^2 - d^2}} & ||p(t) - p_d(\gamma)|| < d \end{cases}, \tag{31}$$

where d is the value for the distance from which the virtual target stops and simply waits for the vehicle to get closer. However, to implement this strategy for the evolution of the virtual target depending only on the distance between the actual vehicle and the target, one has to account for noisy position measurements either from odometry or the Global Positioning System (GPS). To do so a first-order system can be used, which ends up filtering the high-frequency noise present in the input, to define $\ddot{\gamma}$,

$$\ddot{\gamma} = -K_V (\dot{\gamma} - \dot{\gamma}_{REF}) \tag{32}$$

VI-A2 UAV Path-following Control Design

By joining this control strategy with a virtual target approach, similar to the one designed for the ASV that selects which reference the vehicle must track, it is possible to perform the PF and also do so in a cooperative scenario. The evolution of the virtual target is defined by a structure equal to (31). However the desired references can be rewritten as a function of the virtual target parameter γ,

$$p_d = p_d(\gamma) \tag{33}$$

$$\dot{p}_d = \frac{\partial p_d(\gamma)}{\partial \gamma}\dot{\gamma} \tag{34}$$

$$\ddot{p}_d = \frac{\partial}{\partial t}\left(\frac{\partial p_d(\gamma)}{\partial \gamma}\dot{\gamma}\right) = \frac{\partial^2 p_d(\gamma)}{\partial \gamma^2}\dot{\gamma}^2 + \frac{\partial p_d(\gamma)}{\partial \gamma}\ddot{\gamma}. \tag{35}$$

which are meant to directly feed the controller defined in equation (18). The terms $\ddot{\gamma}$ and $\dot{\gamma}_{REF}$ are defined as in (32) and in (31) respectively.

VI-A3 Cooperation between ASV and UAV

The chosen strategy to ensure CPF is inspired in [4]. Although in the present case, the method is applied to two vehicles only, we present the results in their general form for a multi-agent graph topology. The communication network between vehicles can be described as a graph $\mathcal{G}(\mathcal{V}, \mathcal{E}, \mathcal{A})$, where $\mathcal{V}$ is a set of nodes, in this case, a set of $n \in \mathbb{N} \setminus \{1\}$ vehicles, also $\mathcal{E}$ defines the edges that connects each node to another, which means that for any ϵ_{ij} it is told that the vehicle i is connected to the vehicle j which is not necessarily guaranteed for the other way around, and the $\mathcal{A}$ is an adjacency matrix that can be weighted. It is also useful to define for each vehicle a vector with the information of which vehicles can send information into the vehicle i, $\mathcal{N}_i^{in}$ and to which vehicles the vehicle i is able to send information, $\mathcal{N}_i^{out}$. Regarding the scenario in study the graph is undirected which means that $\mathcal{N}_i^{in} = \mathcal{N}_i^{out}$. It is also useful to talk about the degree matrix, D, which is a diagonal matrix that tells how many edges are connected to each node. The Laplacian matrix is defined as $L = D - \mathbb{A}$.

The goal is to create a control law for correction of $\dot{\gamma}$, defined as $v^c = [v_1^c, \dots, v_N^c]^T$ for each vehicle i, with $i \in \mathbb{N}$. This law has to bring $|\gamma_i - \gamma_j| \to 0$, $\forall j \in \mathcal{N}_i^{in}$, and therefore, $\dot{\gamma}^c \to 0$ when all γ values, the considered state for the vehicles, are equal. The first step is to define the error vector as $\xi = [\xi_1, ..., \xi_N]^T$, which is given by

$$\xi_i = \sum_{j \in \mathcal{N}_i^{in}} a_{ij}(\gamma_i - \gamma_j), \tag{36}$$

this can be represented more compactly as,

$$\xi = L\boldsymbol{\gamma}, \tag{37}$$

where L is the Laplacian matrix and $\boldsymbol{\gamma}$ is a vector that represents the state of each vehicle i regarding the value of γ, $\boldsymbol{\gamma} = [\gamma_1, \dots, \gamma_N]^T$. The proposed control law for v_i^c can be written as,

$$v_i^c = -k_i \sum_{j \in \mathcal{N}_i^{in}} a_{ij}(\gamma_i - \gamma_j), \tag{38}$$

and in compact form as,

$$v^c = -K\xi = -KL\boldsymbol{\gamma}, \tag{39}$$

where $0 < K \leq 1$ is a proportional gain. This control law yields

$$\dot{\boldsymbol{\gamma}}^{\boldsymbol{c}} = \dot{\boldsymbol{\gamma}} + v^c, \tag{40}$$

where $\dot{\boldsymbol{\gamma}}^{\boldsymbol{c}} = [\dot{\gamma}_1^c, \dots, \dot{\gamma}_N^c]^T$ are the corrected virtual targets speed.

A diagram representing the control structure that is going to be implemented in the following section to accomplish the cooperative mission between the marine and the aerial vehicle connected by a tether is included in figure 11.

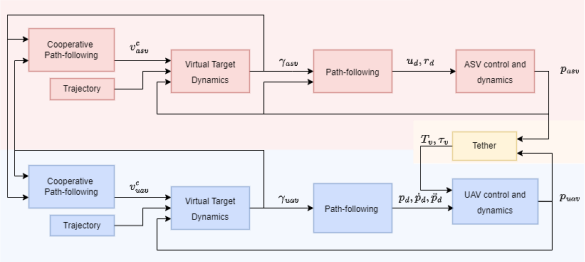

Fig. 11: Final CPF architecture.

VII. Cooperative System Simulation

VII-A. Cooperative Mission between an ASV and an UAV linked by a Tether

The cooperative mission is the combination of the previous individual missions, a lawn-mowing path with a relative shift of $[x, y, z] = [3, 3, 9]\,m$, which means that $\Delta z/\Delta x \approx 2.1213$, with both vehicles connected by a tether which is a considered disturbance on the UAV. There is a constant wind disturbance of $[-2, 0, 0]\,N$. To study the impact of sea ondulation it is added to the ASV an height periodic variation, a sine wave with amplitude of $20\,cm$ and a frequency of $0.2\,Hz$. Noise is introduced in the positions of both vehicles in order to test the robustness of the entire system, it is gaussian noise with mean $0\,m$ and standard deviation of $0.25\,m$, $\mathcal{N}(0, 0.25)$. The UAV starts at $[x, y, z] = [1, 1, 2]$m and the ASV at $[x, y, z] = [-2, 0.5, 0]\,m$. The selected gains for the outer-loop of the UAV controller from (18) are $K_P = 1.5$, $K_I = 0.2$ and $K_D = 1.5$. For the inner-loop of the UAV controller from (21) are $K_P = 10$ and $K_D = 10$. The selected gains for the control laws of the ASV from (28) and (29) are $K_P = 1$ for the surge speed and $K_P = 10$ for the yaw-rate, and also $K_I = 0.2$ for both laws. The path for each vehicle is the same but now there is a continuous CPF algorithm making both vehicles wait for each other while following their own paths. The value selected for K and L from (40) are

$$K = \begin{bmatrix} 1 & 0 \\ 0 & 1 \end{bmatrix} \quad , \quad L = \begin{bmatrix} 1 & -1 \\ -1 & 1 \end{bmatrix}. \tag{41}$$

The threshold distance that defines whether the virtual target moves or not is kept at 5 m for both vehicles. Also the gain for the dynamic presented in (32) is $K_V = 1$ for both vehicles. A representation of the cooperative mission in which both vehicles follow their path along with each other is illustrated in figure 12. It is also represented the virtual target of each vehicle at each given instant of time.

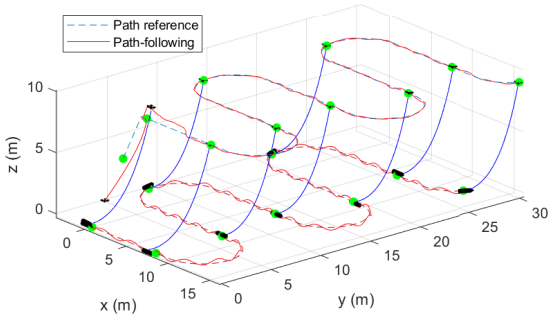

Fig. 12: Cooperative Mission with tether.

Regarding the CPF algorithm it can be seen in figure 13 that $\dot{\gamma}_{uav}$ and $\dot{\gamma}_{asv}$ behave as expected by converging to 1, which means that both vehicles successfully converge to its own virtual target and are able to keep following it, as well as that their virtual targets are also following each other with similar values for γ, achieving cooperation.

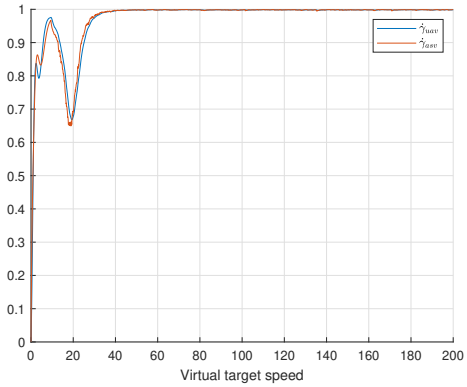

Fig. 13: Cooperative Mission - Virtual target speed $\dot{\gamma}$ for each vehicle.

The evolution of the tether length and departure angle is shown in figures 14 and 15.

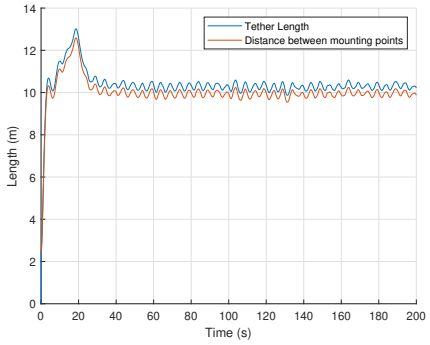

Fig. 14: Cooperative Mission - Tether Length.

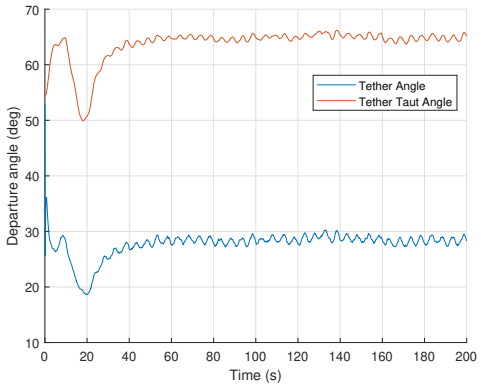

Fig. 15: Cooperative Mission - Tether departure angle at the ASV mounting point.

VII-B. ROS Simulation - a new Tether Plugin

One of the main contributions of this work is a Gazebo Plugin to include the tether in simulation in a ROS environment. This environment was developed by the Dynamical Systems and Ocean Robotics Laboratory (DSOR) and further adapted to a similar scenario in [6]. It runs in Ubuntu 18.04LTS and with ROS Noetic [2]. To perform the simulations it was used Gazebo which is a three-dimensional (3D) simulator that runs a physics engine. Three plugins were used in this simulation, the UUVSimulator Plugin [7], the PX4 SITL Gazebo Plugin [1] and the tether Plugin.

The tether Plugin is basically a discretization of the equation (1) which gives the altitude of any point in a catenary given the horizontal span of that point from the ASV mounting point, the tether length, computed by the polynomial fit from (12) and the relative position between the two extremities of the cable. The tether is composed by a fixed number of joints and links, each joint is a point in the catenary which is connected by a straight link that dynamically stretches and shrinks to the distance between each of those joints through the whole simulation. The bigger number of joints and links used the more realistic the

simulation may look, however it is important to clarify that each of these pairs are a body that the simulator has to render therefore the increase of bodies may overload the whole system. The plugin also computes and applies the force and torque which are being exerted on the UAV. The impact of the tether on the ASV is neglected because it is considered residual. The aerodynamic effects are also ignored. The full system, which is the two vehicles attached by the tether is presented in figure 16. The mounting points of the tether are virtually above and below the ASV and UAV respectively.

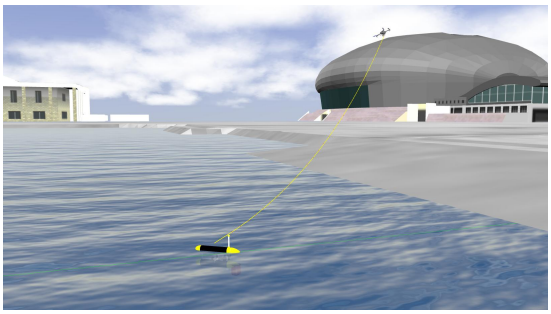

Fig. 16: Gazebo Simulation - full system the UAV, ASV and the tether.

VIII. Conclusion and Future Work

VIII-A. Conclusion

This thesis seeks to include in a scenario of a cooperative mission between an aerial vehicle and a marine vehicle a tether that connects them. In Section II this problem is addressed by first modelling the cable as a catenary and then creating a polynomial approximation for the desired length for a given relative position between vehicles. In Sections IV and V it was defined the notation and the modelling of each type of vehicle and then two control strategies were specified. For the UAV it was developed an inner-loop outer-loop strategy, the inner part was meant to follow orientation references while the outer part was to track position, linear velocity and acceleration. For the ASV it was used two inner-loops to track references for the surge speed and the yaw rate. Section VI starts by outlining the individual PF strategy for each vehicle by designating a virtual entity to be followed. Then the cooperation was specified as a correction of the virtual targets speed in order to get the targets synchronized in each of their own paths. Lastly, in Section VII the results are demonstrated with regard to a generic lawn-mowing path. All of these were conducted in a MATLAB environment. The system overall behaved as desired for this specific system when working in a well chosen working zone. The Section ends with the presentation of a new tether plugin for Gazebo.

VIII-B. Future Work

The work developed for this master's dissertation can pave the way for new research and developments regarding this topic. Some of those topics are listed below.

- Implementation of the pulley capable of tracking a reference for the tether length based on the polynomial fit developed in (12).
- To study the tethers available and which ones would fit such missions, to do not treat this cable only as a theoretical entity.
- To develop tether plug-in to include a more complex model for the tether, including aerodynamic effects and others, with the ultimate goal to make it as realistic as possible.
- To specify and study the mechanisms related to the take-off, landing of the UAV as well as safety measures regarding any undesired and possibly harmful actions by any intervening part of the system.
- To migrate the system to a more constrained environment, for example with some obstacles to avoid.

References

[1] PX4 Autopilot User Guide. https://docs.px4.io/main/en/. visited in 6/10/2022.

[2] ROS Noetic. https://www.ros.org/. visited in 14/10/2022.

[3] A. P. Aguiar and A. M. Pascoal. Dynamic positioning and way-point tracking of underactuated auvs in the presence of ocean currents. 41st IEEE Conference on Decision and Control, December 2002.

[4] R. Ghabcheloo, A. P. Aguiar, A. Pascoal, C. Silvestre, I. Kaminer, and J. Hespanha. Coordinated path-following in the presence of communication losses and time delays. SIAM Journal on Control and Optimization, 48:234–265, 2009.

[5] P. G. Ioppo. The design, modelling and control of an autonomous tethered multirotor uav. Master's thesis, University of Stellenbosch, March 2017.

[6] M. Jacinto. Cooperative motion control of aerial and marine vehicles for environmental applications. Master's thesis, Instituto Superior Técnico, December 2021.

[7] M. M. M. Manhães, S. A. Scherer, M. Voss, and L. R. Douat. Uuv simulator: A gazebo-based package for underwater intervention and multi-robot simulation. IEEE, 2016.

[8] D. Mellinger and V. Kumar. Minimum snap trajectory generation and control for quadrotors. 2011 IEEE International Conference on Robotics and Automation, May 2011.

[9] R. M. Murray, Z. Li, and S. S. Sastry. A Mathematical Introduction to Robotic Manipulation. 1994.

[10] J. Ribeiro. Motion control of single and multiple autonomous marine vehicles. Master's thesis, Instituto Superior Técnico, October 2011.

[11] K. A. Talke. Hanging Tether Management for Unmanned Air-Surface Vehicle Teams. PhD thesis, UC San Diego, 2021.

[12] K. A. Talke, M. de Oliveira, and T. Bewley. Catenary tether shape analysis for a uav - usv team. 2018 IEEE RSJ International Conference on Intelligent Robots and Systems (IROS), October 2018.

[13] F. Vanni, A. P. Aguiar, and A. M. Pascoal. Cooperative path-following of underactuated autonomous marine vehicles with logic-based communication. IFAC Proceedings Volumes, 41:107–112, 2008.